Coupled fluctuations of blood pressure and heart rate time series

Isla Gilmour

Exeter College

Dissertation submitted in partial fulfillment of the requirements for the degree of Master of Science in Mathematical Modelling and Numerical Analysis at the University of Oxford

September 1995

Acknowledgments

I would like to thank Dr. A.C. Fowler for suggesting the topic of this dissertation and for his guidance, Dr. G. Kember for the help and encouragement he gave me during the research and Dr. J.D. Young for providing the data needed to make this dissertation possible. I would also like to thank the Engineering and Physical Sciences Research Council for their funding throughout the year. Finally, thanks to my parents for their unending support throughout my education.

Abstract

The human cardiovascular system governs the heart rate and blood pressure. A neural sensor called the baroreceptor is controlled by the the blood pressure; the sensitivity of its reflex is important in determining the cause of hypertension. This sensitivity may be obtained from the coupled fluctuations of blood pressure and heart rate time series. However, the current method used assumes locally linear coupling of the heart rate and blood pressure, which has been shown to be nonlinear. In this dissertation we apply this current method to sample data, investigate improvements and, having gained further insight into the cardiovascular system from models of the system, offer an alternative method of measuring the baroreceptor relex sensitivity.

Contents

List of Figures

Chapter 1

Introduction

Measuring a physical characteristic of a system over a period of time generates a sequence of observations, either continuous or discrete, known as a time series. Time series arise in a wide variety of fields, varying from share prices, electricity consumption for a region, hourly traffic density on a stretch of road to a time series recording the electrical activity of the brain, measured by an electroencephalograph. Often these time series are used to predict future values, *e.g.* advising when to buy or sell shares. In other cases the time series contains information which is important in diagnosing the state of the system. The use of a time series of respiratory output to aid in the diagnosis of Cheyne-Stokes respiration, a respiratory irregularity in adults, is one of the earliest examples of the use of time series to aid diagnosis in the medical field [11]. More recently plethysmograms, the output of a combined pulse and respiratory monitor, have been used to diagnose the degree of risk to a child of sudden infant death syndrome (cot death) [7]. Here we investigate the use of heart rate and blood pressure time series to aid in the diagnosis of the cause of hypertension in patients.

1.1 Hypertension

Hypertension is the clinical name for high blood pressure which may be due to a number of widely differing causes. Patients with different causes of hypertension may have very similar symptoms, which make diagnosis difficult. Those in most danger from hypertension are often suffering from other maladies and are in intensive care units.

The cardiovascular system (CVS) controls the blood pressure by altering the heart rate and compliance (*i.e.* elasticity) of the blood vessels. An increase in blood pressure triggers pressure detectors, known as baroreceptors, which send signals through nerves to the central nervous system. This causes the heart rate to decrease and the compliance to increase, thus decreasing the blood pressure. The coupling between the blood pressure

(BP), heart rate (HR) and compliance (C) via the reflex of the baroreceptor (BR) is stronger than the coupling between the heart rate, compliance and blood pressure due to other regulatory mechanisms, as illustrated in fig. 1.1.

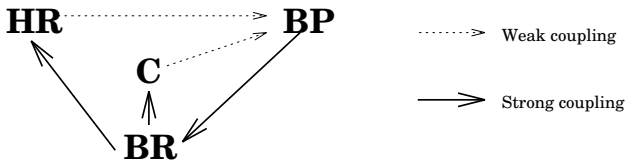

Figure 1.1: Coupling of the CVS

The strength of the signal emitted by the baroreceptor varies according to the blood pressure, increasing strength with increasing blood pressure, and between individuals. A general trend is that the baroreceptor of a healthy young person will have a large change in signal strength for small changes in blood pressure, while a healthy old person will have little change in signal strength for large changes in blood pressure [10]. As a result the heart rate of the young person varies considerably in response to the signal in order to maintain a small variation in blood pressure, while the older person has insufficient variation in heart rate, causing larger variation in blood pressure. The sensitivity of the carotid sinus baroreceptor, known as the baroreceptor reflex sensitivity (BRS), largely determines the strength of signal emitted in response to variation in blood pressure. We wish to determine this baroreceptor reflex sensitivity as it is this which aids doctors in diagnosis of the cause of hypertension. Of the four major components of the CVS considered (blood pressure, baroreceptor reflex, compliance and heart rate), heart rate and blood pressure may be measured non-invasively.

1.2 Blood pressure and heart rate time series

Heart rate is obtained by analysing electrocardiograms (ECGs), which are traces of the electrical activity of the heart measured by means of three devices attached to the right arm, left arm and left leg of the patient. The output from these devices is of a typical amplitude of the order of 1 mV, which is amplified to give an ECG with typical amplitude of the order of 1 V. A section of an ECG is shown in fig. 1.2.

Each heartbeat contains five distinctive phases, P, Q, R, S and T, which are distinguishable on the ECG. The P part of the waveform is the natural pacemaker firing, the QRS section represents the wave of electrical activity as the heart muscle depolarises and contracts, with T representing repolarisation. The R peak is chosen as a reference

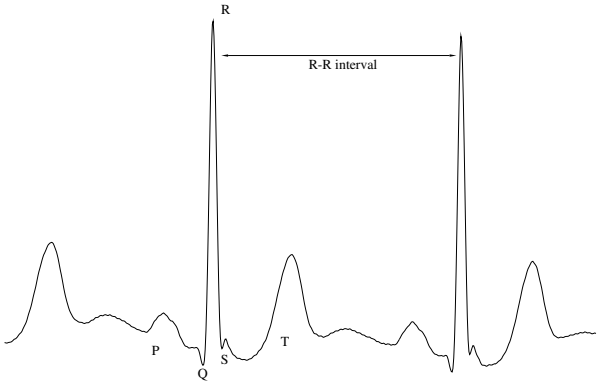

Figure 1.2: Example of an ECG section

point as it is usually the most definite and distinct characteristic of the output. The interval between R peaks is known as the R-R interval, from which the heart rate, 1/(R-R interval) may be calculated.

The blood pressure is measured using a device inserted into the radial artery, a blood vessel in the wrist. The device consists of a pressure gauge which amplifies the change in pressure to give output as in fig. 1.3.

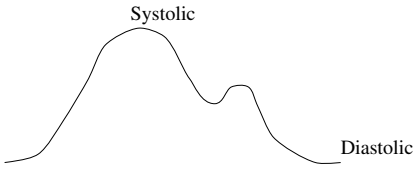

Figure 1.3: Example of blood pressure output

The systolic pressure is the maximum pressure attained during a heart beat and corresponds to the effect of the contraction of the heart reaching the blood vessel. The diastolic pressure is the minimum pressure attained during a heart beat, corresponding to the relaxed phase of the heart beat. The blood pressure at the systolic point of the trace is taken as the reference since it is the most distinct feature in the majority of cases.

ECG and blood pressure output are stored on analogue tape which is then sampled at a frequency of 256 Hz, using peak detectors to locate the R peaks and systolic pressure values. A heart rate time series is formed by taking the heart rate, calculated from the previous R-R interval, as the data for all sampling points which fall in the present heart beat, as shown in fig. 1.4.

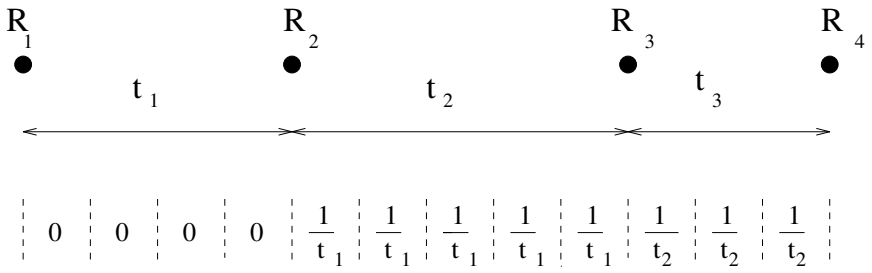

Figure 1.4: Forming a heart rate time series

From the blood pressure output the systolic blood pressure value is taken as the data for all sampling points between that peak and the next to form a blood pressure time series, as shown in fig. 1.5.

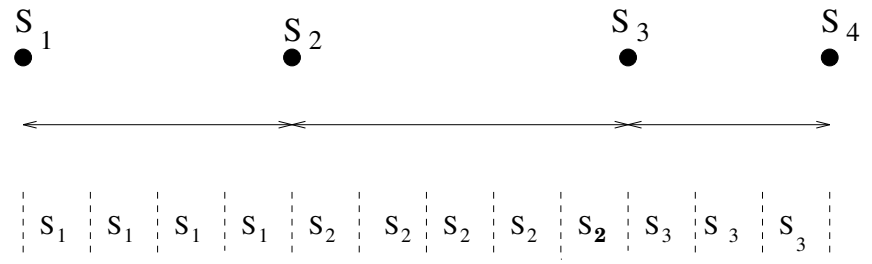

Figure 1.5: Forming a blood pressure time series

Data is from both pre-operative patients and willing volunteers in normal health. Heart rate in a healthy person is typically 75 beats per minute (BPM) while systolic blood pressure is typically 120 mmHg.

1.3 Baroreceptor reflex sensitivity

We have established that we wish to measure the variation in the strength of the signal emitted by the baroreceptor reflex in response to variation in the systolic blood pressure, known as the baroreceptor reflex sensitivity (BRS), and used to aid diagnosis. We are able to form heart rate and blood pressure time series from measurements taken from a patient. Now we consider different ways of using these time series to obtain an estimate of the BRS. Since we are able to measure the heart rate and blood pressure and wish to

find the baroreceptor reflex sensitivity let us consider a simplified version of the CVS as shown in fig. 1.6.

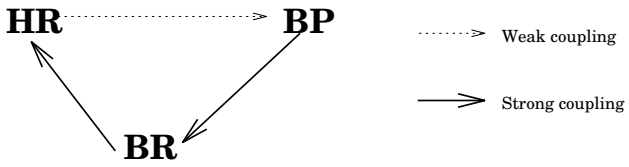

Figure 1.6: Simplified coupling of the CVS

If we can increase the blood pressure without directly affecting the heart rate then any change in the heart rate will be due to the coupling via the baroreceptor reflex. Injecting a patient with a pressor drug (phenylephrine) decreases the diameter of the blood vessels, thus increasing the resistance, which increases the blood pressure without directly affecting the heart rate [15]. The CVS works through the weak coupling to reduce the blood pressure to a normal level. From the data obtained during this procedure one may plot the R-R intervals against the increasing blood pressure. Fitting a straight line to the points, using linear regression, the gradient of the line is the ratio of response in heart rate to change in blood pressure. Traditionally this is taken as an approximation of the BRS. While this method gives the information desired it is not a practical solution since the administration of pressor drugs is undesirable, and repetitive administration is medically not viable. This motivates the search for a way of determining the sensitivity of the system to the baroreceptor reflex using non-invasive techniques, *i.e.* by using the natural fluctuations in the heart rate and blood pressure systems.

Suppose the coupling between the blood pressure and heart rate, via the baroreceptor reflex, is linear. Then the linear relation between heart rate and blood pressure will be preserved by taking Fourier transforms of the time series. The advantage of transforming the data into the frequency domain is that the signal emitted by the baroreceptor reflex in response to change in blood pressure is known to be of a frequency in the range 0.05-0.15 Hz [15]. In chapter two we look at the method which is currently used. It assumes that the coupling between the heart rate and blood pressure is linear and manipulates the data to find an approximation to the BRS. The coupling between the heart rate and blood pressure is nonlinear, as has been shown by Eckberg [6], suggesting that a method relying on linear coupling is not ideal. Before proceeding further we consider a simple discrete model of the CVS, developed by deBoer, Karemaker and Strakee [5], in order to gain a better understanding of the system.

A generalisation of the Fourier analysis method described above is explained in chapter three. It uses singular value decomposition (SVD) as developed by Broomhead and King [4], which improves the results obtained. In chapter four we develop a more complicated continuous model of the CVS designed by Madwed et al. [12]. The further insight into the system which this provides enables an alternative method of approximating the BRS to be constructed, which is tested on real data. Finally in chapter five we discuss the conclusions which can be drawn from the results obtained.

Chapter 2

Fourier techniques and a discrete model of the cardiovascular system

2.1 Fourier techniques

We established in sections 1.1 and 1.2 that we wish to find the baroreceptor reflex sensitivity, and that we are able to measure heart rate and blood pressure. The method currently employed [15] relies on Fourier techniques. Heart rate and blood pressure time series obtained by the sampling method explained in section 1.2 are then re-sampled at a chosen frequency, f_S, in order to decrease the amount of data needed while retaining enough detail in the data to enable analysis.

2.1.1 Aliasing and leakage

The Fourier transform of a continuous signal $x(t)$ is given by

$$\bar{x}(t) = \int_{-\infty}^{\infty} x(t) \exp(2\pi i f t) dt \tag{2.1}$$

We wish to apply a discrete version of this transform to a discrete N point time series $\xi(t) = \{\xi_1, \xi_2, \ldots, \xi_N\} = \{\xi_k\}_{k=1}^{N}$ where $\xi_k = \xi(t_0 + k\delta)$ and δ is the sampling interval. Problems can arise due to the finite number of sampling points. Consider a sine wave of frequency 1 Hz. Let us represent this sine wave by two time series formed by using sampling intervals $\delta_\alpha = 1$ and $\delta_\beta = 1/2$, both with $t_0 = 1/4$. Then

$$\alpha(t) = \{1, 1, 1, \ldots\}$$

$$\beta(t) = \{1, -1, 1, -1, \ldots\} \tag{2.2}$$

Simple observation shows that the frequency of the time series $\{\alpha_k\}$ is zero while that of the time series $\{\beta_k\}$ is 1 Hz. The frequency of $\{\alpha_k\}$ fails to reflect that of the signal, the 1 Hz sine wave, from which it was derived due to the phenomenon of any frequency lying outside the range $(-f_c, f_c)$ spuriously being moved into that range, where f_c is the *Nyquist critical frequency* [14] given by

$$f_c \equiv \frac{1}{2\delta} \tag{2.3}$$

This is an example of *aliasing*, the spurious moving of frequencies into different ranges. To avoid this phenomenon we need to choose δ such that

$$\begin{aligned} f_c &\geq f_S \\ \Rightarrow \delta &\leq \frac{1}{2f_S} \end{aligned} \tag{2.4}$$

to construct a time series from a signal of frequency f_S.

In the case of heart rate and blood pressure we do not expect any oscillations in the data to have a frequency greater than that of the heart beat. A typical value of the R-R interval is 800 ms, giving a typical heart beat frequency of 1.25 Hz. Re-sampling at a rate of 4 Hz. satisfies the criterion in eqn. 2.4 for fluctuations of R-R interval down to 400 ms, and so we choose the re-sampling frequency, f_S, of 4 Hz.

Due to the limited number of sampling points in the time series there is *leakage* from one frequency range into neighbouring ranges when calculating the power spectra. In order to limit this effect of leakage the heart rate and blood pressure time series, which typically consist of 500 sampling points, are interpolated to 512 points, desirable in order to use a fast Fourier transform algorithm, an efficient method of applying a discrete Fourier transform to the time series. If the time series is padded with zeros it causes an increase in power near the origin, which leaks into the neighbouring ranges contaminating the data in which we are interested.

When calculating a discrete power spectrum we are effectively applying a square window to an infinite sequence, with the window zero except over the N data points of the time series, where its value is one. This window varies rapidly at the endpoints of the time series which causes leakage at larger frequencies. This may be remedied by applying a window which varies less rapidly at the extremes of the time series, *e.g.* a *Hanning window* [13], which modifies the data at point j of an N point time series by a factor w_j, given by

$$w_j = 0.5 * \left[1 - \cos\left(\frac{2\pi j}{N}\right)\right] \tag{2.5}$$

2.1.2 Description of Fourier technique method

Having interpolated the data and applied a Hanning window, we set the mean of each time series to zero and then take the discrete Fourier transform [14] which maps the time series $\xi(t) = \{\xi_k\}_{k=1}^{N}$, with sampling interval δ, from time space into the frequency domain by

$$\bar{\xi}(f_n) = \delta \sum_{k=0}^{N-1} \xi_k \exp\left(\frac{2\pi i k n}{N}\right) \tag{2.6}$$

Any linear relation between the two time series in time space is preserved in mapping to the frequency domain by this transformation. The power of a frequency, $P(f_n)$, is then estimated, for N even, by

$$P(f_n) = \left| \sum_{k=-N/2}^{N/2-1} \xi_k \exp(2\pi f_n k \delta) \right|^2 \tag{2.7}$$

[14] from which a power spectrum, a plot of power against frequency, may be constructed.

Returning to the example of the time series derived from the sine wave signal from section 2.1.1, β_k, the time series with $\delta = 1/2$, has a power spectrum consisting of a concentrated peak at 1 Hz. Thus, for simple systems, we are able to identify the frequency of the signal from which the time series is derived from the power spectrum. This is useful when we do not know what is causing the original signal, as in the case of heart rate and blood pressure.

The baroreceptor reflex responds to the blood pressure by emitting signals which affect the heart rate. The processing of the time series by the method described above is motivated by the knowledge that these emitted signals have frequencies in the range 0.05-0.15 Hz [15, 16]. By transforming the data into the frequency domain this additional information is made available. The method proceeds by calculating the 'gain' for each frequency, defined as

$$\text{gain}(f) = \frac{\text{heart rate power}(f)}{\text{systolic blood pressure power}(f)} \tag{2.8}$$

If we assume that the heart rate and blood pressure are linearly coupled then we may use the preservation of linear relations by the Fourier transformation to obtain a measure of the ratio of heart rate to blood pressure. Since, for a given time series $\xi(t)$, $P(f_n) \propto |\xi|^2$ then

$$gain(f) = \frac{P_\phi(f)}{P_\psi(f)} \propto \left|\frac{\phi}{\psi}\right|^2 \tag{2.9}$$

where ϕ = heart rate and ψ = blood pressure.

Taking the power at each frequency as a N point frequency series, we may calculate the correlation, r, between the heart rate and blood pressure power, given by

$$r = \frac{\frac{1}{(N-1)} \sum_{i=1}^{N} (\phi_i - \mu_\phi)(\psi_i - \mu_\psi)}{\sigma_\phi \, \sigma_\psi} \tag{2.10}$$

with ϕ_i = heart rate power at point i, ψ_i = blood pressure power at point i, μ_a = mean of the N point series a and similarly for σ_a = standard deviation [2]. In order to have a measure of local linearity we consider the correlation of frequency f_j, r_j, as the correlation of the five point series consisting of the five values centred about point j, *i.e.*

$$r_j = \frac{\frac{1}{4} \sum_{i=-2}^{2} (\phi_{j+i} - \mu_{\phi_j})(\psi_{j+i} - \mu_{\psi_j})}{\sigma_{\phi_j} \, \sigma_{\psi_j}} \tag{2.11}$$

If the coherence, r_j^2, at a point exceeds 0.5 then the point j is defined as being sufficiently linear for the above relation for the gain, eqn. 2.9, to hold [15].

We wish to use this measure of 'gain' in order to estimate the sensitivity of the baroreceptor reflex. The frequencies of the signals emitted in response by the baroreceptor reflex are known to be in the range 0.05-0.15 Hz [15, 16]. The average value of the gain over this range is accepted as an estimate of the BRS if the coherence within this range exceeds 0.5 [15].

2.1.3 Pre-processing of data

On plotting the re-sampled data it was found that artifacts existed in some of the blood pressure data, *e.g.* that for patient 5 as shown in fig 2.1. These are due to the way the

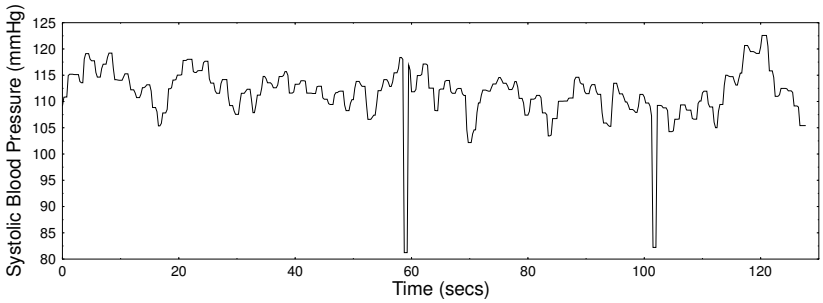

Figure 2.1: Original data with artifacts

systolic peaks are detected in the blood pressure output. Although there are only a small number of these, they may alter the results considerably due to their large deviation from the mean value. In order to correct these artifacts we compare the blood pressure and heart rate values, which typically retain the same value for several points. Using

the blood pressure values before and after the artifact we are able to replace the blood pressure values during the artifact with either the proceeding or the following values, chosen so that the change in blood pressure coincides with that in the heart rate.

2.1.4 Results

The heart rate and blood pressure time series in fig. 2.2 below are from pre-operative patients in a supine state, *i.e* lying quietly. From these figures we can see that there are fast time oscillations in the data over 3-7 seconds, which are due to respiration. Long term oscillations over $\sim$ 60 seconds are clearly visible in the data from patient 6, fig. 2.2 (e), and are low frequency variations due to mechanisms in the body which respond to adjust to changes in surroundings [15]. The oscillations over $\sim$10 seconds are known as 10 s Mayer waves, most clearly seen in patient 5, fig. 2.2 (c) & (d), and are mid-frequency variations caused by the effects on heart rate of the baroreceptor reflex response. Due to the weak coupling between heart rate and blood pressure these effects are also seen in blood pressure. One can also see that the heart rate and blood pressure are out of phase.

The presence of these three distinct frequencies of oscillation is more clearly illustrated in the power spectra in fig. 2.3. The long term oscillations give rise to a definite peak at $\sim$ 0.02 Hz, seen clearly in fig. 2.3 (e). A second peak, centred about 0.3 Hz, is due to respiration with the Mayer waves causing a third distinct peak at 0.1 Hz. Smaller peaks are spread throughout the frequency range due to noise in the data, present in the patient's system and introduced when recording the data.

The plots of gain, fig. 2.4, are rapidly varying, as is to be expected when taking the ratio of two small numbers with large variation. Plots of coherence, fig. 2.4 show that the values of coherence are small for all data, and none exceed the required 0.5 level in order to assume local linearity over the required range.

The values obtained for coherence demonstrate that the heart rate and blood pressure time series cannot be assumed to be locally linear, and so this method fails to find an acceptable approximation to the baroreceptor reflex sensitivity, BRS. Even if the time series are linearly coupled and yield a coherence of one, the use of the average gain over the range 0.05-0.15 Hz as an approximation to the BRS is not obviously justified. We now seek to gain further understanding of the cardiovascular system (CVS) in order to investigate the justification of this method.

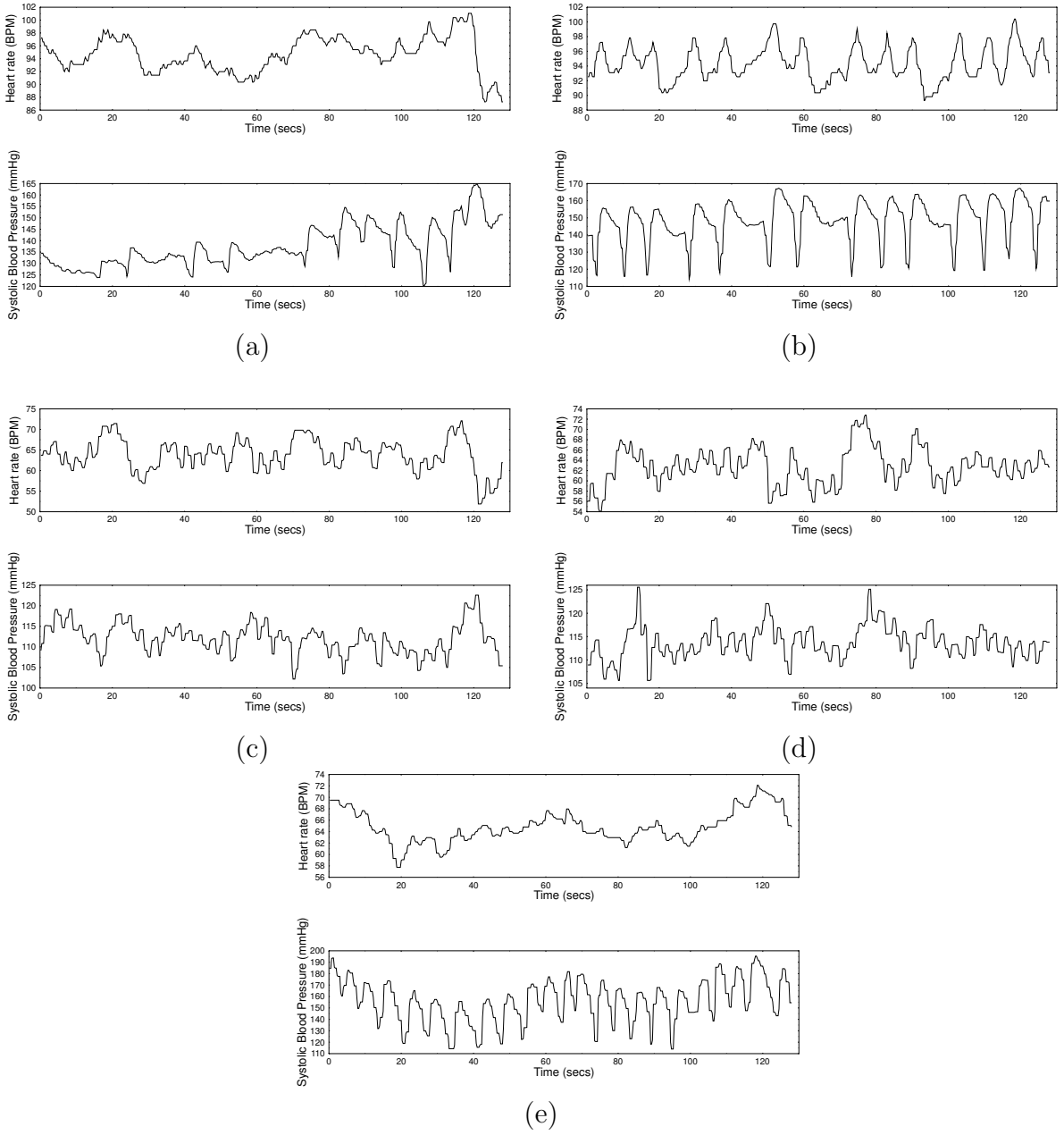

Figure 2.2: Original data (a) patient 4(1), (b) patient 4(4), (c) patient 5(1), (d) patient 5(2) and (e) patient 6

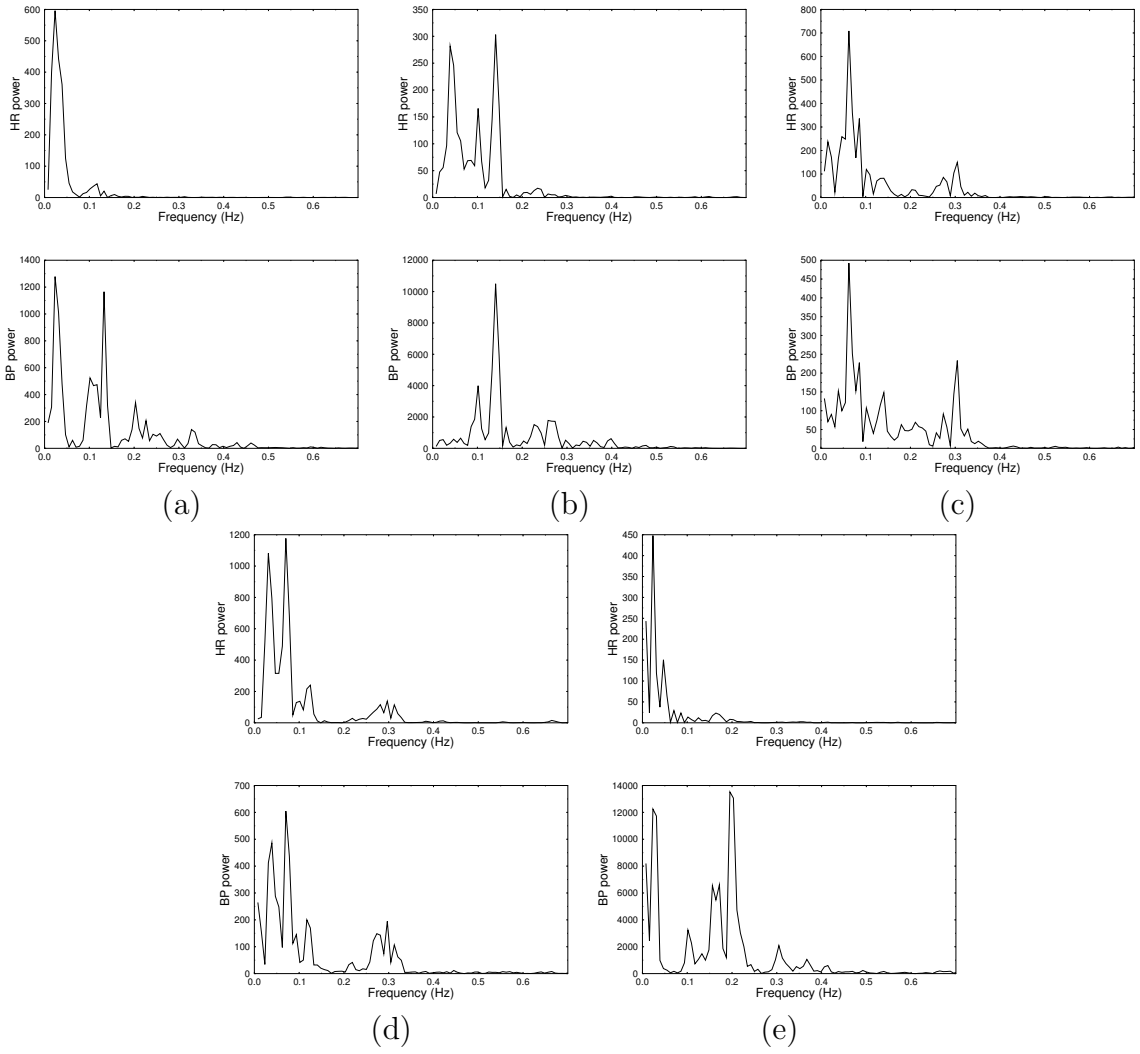

Figure 2.3: Power spectra of original data (a) patient 4(1), (b) patient 4(4), (c) patient 5(1), (d) patient 5(2) and (e) patient 6

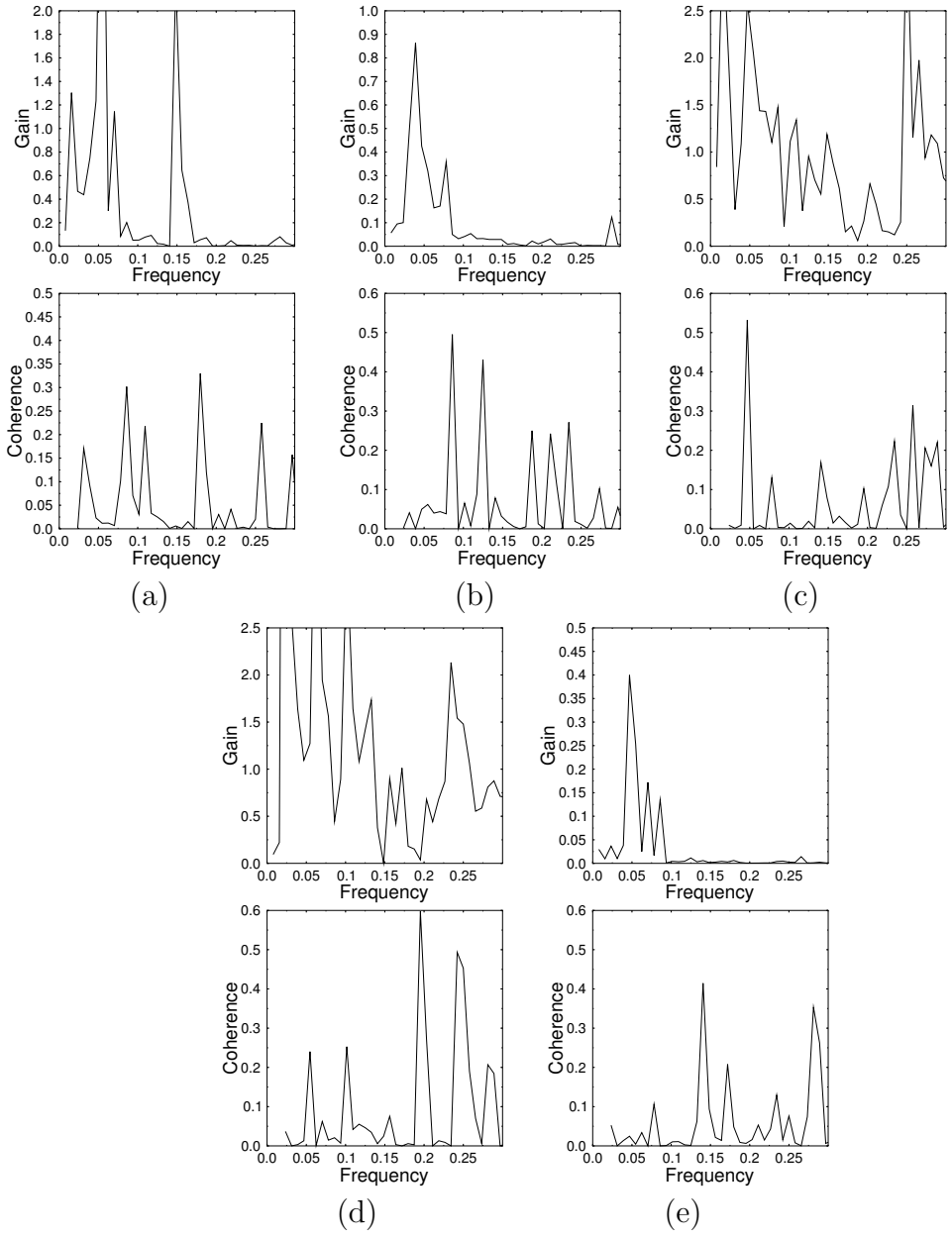

Figure 2.4: Gain and coherence of original data (a) patient 4(1), (b) patient 4(4), (c) patient 5(1), (d) patient 5(2) and (e) patient 6

2.2 Discrete model of the cardiovascular system

We wish to find what drives the cardiovascular system and how the different components affect one another in order to be able to understand what the baroreceptor reflex affects, and what it is affected by. It is not possible to isolate different parts of the system in the patient and we do not know how all of the parameter values change, so we turn our attention to a model of the system. This has the advantage that noise, inherent in experimental data, may be omitted. The parameter values may also be varied and the response of the system to different values found. A model has the disadvantage that, unless it is so complex that it is no longer easily understood, it is not able to take account of all the influencing factors. However, a good model taking account of the most important factors will enable us to increase our understanding of the system, and in particular of the baroreceptor reflex sensitivity.

2.2.1 Formulating a model

In order to formulate a model we need to decide which parts of the cardiovascular system are important, and hence need to be included in the model of the system. The discussion above (see section 1.3) suggests that the heart rate and systolic blood pressure need to be included, and that the affect of the baroreceptor reflex needs to be incorporated in some way. We know that there is a weak coupling between heart rate and blood pressure via other regulatory mechanisms, and that the baroreceptor reflex responds to blood pressure, affecting the heart rate. Appealing to medical knowledge of how the baroreceptor is incorporated into the cardiovascular system [5], we find that the baroreceptor reflex reacts to the systolic blood pressure directly, and that the response of the reflex is the emission of signals which travel to the central nervous system. Here the incoming signals induce signals in three nerves: the vagal nerve, which transmits the signal rapidly, and a pair of sympathetic nerves which transmit the signal more slowly. The vagal and $\beta-$sympathetic nerves are linked to the cardiac pacemaker which determines when a contraction of the heart occurs, and hence controls the R-R interval. The $\alpha-$sympathetic nerve signal affects the compliance (elasticity) of the blood vessels. As we are interested in the short term variations in the cardiovascular system and our discrete measurements may be taken at most every heart beat we look at a discrete model by deBoer, Karemaker and Strakee [5]. The model consists of difference equations which have as their time interval the duration of a heart beat, and is called a beat-to-beat model.

2.2.2 Description of beat-to-beat model

This model is based on five variables, two of which are the systolic blood pressure and R-R interval used above. In order to incorporate compliance, C, which varies between blood vessels and also within single blood vessels, a single variable is used. The model differentiates between systolic, S, diastolic D and pulse pressure, P, which is the difference between systolic and diastolic pressures. The model is comprised of five equations, with S_n the nth value of systolic pressure *etc.*, which are interdependent in such a way as to form a closed system, as shown in fig. 2.5.

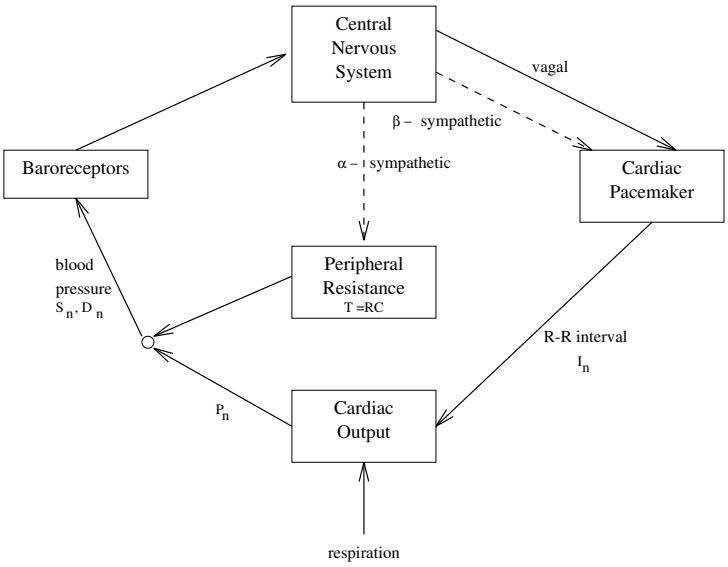

Figure 2.5: Closed loop system of the beat-to-beat model

Baroreceptor response

Consider the reaction of the baroreceptor reflex to differing blood pressure. If the systolic blood pressure is very low then the reflex ceases to react, hence there is a minimum threshold of no reaction. As the systolic pressure increases the reaction of the reflex gradually increases, until the pressure approaches its critical value, at which point the reaction of the reflex becomes much stronger. As the pressure increases beyond this critical value the increase in reactivity levels off as maximum reaction rate is reached, giving an upper threshold. The change in reaction of the reflex in response to the change in systolic pressure may be represented by a sigmoidal response curve (see fig 2.6). As

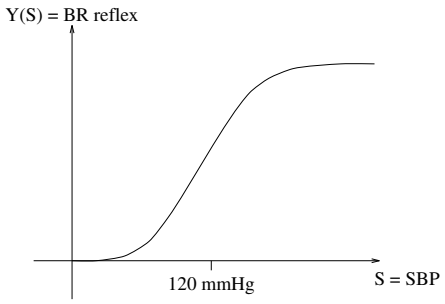

Figure 2.6: Effective systolic pressure

the strength of reaction of the reflex is of more importance than the actual systolic pressure, we define the *effective systolic pressure* as

$$\hat{S}_n = Y(S_n) \tag{2.12}$$

where $Y(S_n)$ describes the sigmoidal response.

Action on cardiac pacemaker

The cardiac pacemaker determines the R-R interval, I_n. It is affected by the signals transmitted by the vagal and $\beta-$sympathetic nerves, which are induced by a signal emitted by the baroreceptor reflex and dependent on the effective systolic blood pressure, $\hat{S}_n$. The vagal nerve transmits the signal rapidly and so the strength of the signal is proportional to the current effective systolic pressure. The $\beta-$sympathetic nerve transmits the signal more slowly, and several preceding values of the effective systolic pressure affect the current strength of signal. Hence the current R-R interval is modelled as an autoregressive function by

$$I_n = a_0\hat{S}_n + \sum_{k>0} a_k\hat{S}_{n-k} + I_0 \tag{2.13}$$

where the a_ks are constants and $\sum_{k>0} a_k = a_0$ so that the total vagal and sympathetic effects are equal. Varying the shape of the weighting function or the ratio of vagal:sympathetic sensitivity is found to have little effect [5].

Action on peripheral resistance

Peripheral resistance is the resistance to blood flow in the vessels, which is controlled by varying the compliance of the blood vessels, and is affected only by the signal transmitted

by the α-sympathetic nerve as a result of the response of the baroreceptor reflex. Given that the resistance, R, and compliance, C, are related by $T = RC$, where T is a time constant, and C is assumed to be constant, we can write the equation in terms of T_n. Using the knowledge that increased pressure causes decreased resistance [5] and modelling the affect of the $\alpha-$sympathetic nerve signal as above we have

$$T_n \,(=\, R_n C) \;=\; T_0 - \sum_{k>0} b_k \hat{S}_{n-k} \tag{2.14}$$

where the b_ks are constants. Taking the effect of the baroreceptor on the peripheral resistance and on the R-R interval to be equal, we use twice the weighting function of that in eqn 2.13, since here we have only sympathetic action, hence $\sum_{k>0} b_k = 2a_0$.

Effect of interval on pulse pressure

The length of the n^{th} interval, I_n, affects the volume of blood which flows into the ventricle. If the preceding interval is long then more blood flows into the ventricle causing a more forceful contraction. This causes the pulse pressure in the next interval to increase. Respiratory forcing is taken by deBoer et al. [5] to act on pulse pressure, causing the addition of simple sinusoidal forcing. However, other sources [1, 10, 16] suggest that the respiratory forcing affects the vagal nerve signal. The deBoer et al. model [5] is

$$P_n = S_n - D_n = \gamma I_{n-1} + P_0 + F \tag{2.15}$$

where F is the respiratory forcing given by $F = A\sin(2\pi f_{resp} \sum_k I_k)$ where A is the amplitude of the forcing, f_{resp} is the frequency of respiration and $\sum_k I_k$ is the time given by the cumulative sum of R-R intervals.

Windkessel equation

The value of the diastolic blood pressure is dependent on the previous systolic pressure due to the properties of the blood vessels [5]. It also depends on the force of contraction, and hence on the previous R-R interval, and on the resistance of the blood vessels, measured via the time constant. The Windkessel model

$$D_n = \frac{D_0}{S_0} S_{n-1} \exp\left\{ -\left[\frac{I_{n-1}}{T_{n-1}} \right] \right\} \tag{2.16}$$

has been found to fit experimental data.

2.2.3 Analysis of model

The above system of equations may be combined to give

$$\begin{aligned} I_n &= a_0\hat{S}_n + \sum_{k>0} a_k \hat{S}_{n-k} + I_0 \\ \hat{S}_n &= Y(S_n) \\ T_n &= T_0 - 2\sum_{k>0} a_k \hat{S}_{n-k} \\ S_{n+1} &= \frac{D_0}{S_0} S_n \exp\left\{-\left[\frac{I_n}{T_n}\right]\right\} + \gamma I_n + P_0 + F \end{aligned} \tag{2.17}$$

This illustrates the closed loop nature of the system, with the current systolic pressure determining the current R-R interval and time constant which together determine the next value for the systolic pressure. Typical values of the parameters are

$$S_0 = 120 \text{ mm Hg} \quad D_0 = 75 \text{ mm Hg} \quad P_0 = 45 \text{ mm Hg}$$

$$I_0 = 800 \text{ ms} \qquad T_0 = 1425 \text{ ms} \qquad \gamma = 0.016 \text{ mm Hg/ms}$$

Let us consider small perturbations d_n, s_n, i_n, τ_n about typical (equilibrium) values D_0, S_0, I_0, T_0. Then we may write the Windkessel equation, eqn. 2.16, as

$$\begin{aligned} d_{n+1} + D_0 &= \frac{D_0}{S_0}(s_n + S_0)\exp\left\{-\left[\frac{i_n + I_0}{\tau_n + T_0}\right]\right\} \\ \Rightarrow d_{n+1} &\sim D_0\left[\frac{s_n}{S_0} - \frac{i_n}{T_0} + \frac{I_0}{T_0}\frac{\tau_n}{T_0}\right] \end{aligned} \tag{2.18}$$

to first order. We notice that the largest two terms balance if

$$\begin{aligned} \frac{s_n}{S_0} &= \frac{i_n}{T_0} \\ \Rightarrow \frac{i_n}{s_n} &= \frac{T_0}{S_0} \end{aligned}$$

$$\approx \quad 10\text{ms/mmHg} \tag{2.19}$$

Considering only the vagal nerve effects we have, from eqn. 2.13

$$a_0 \approx 10\text{ms/mmHg}$$

so choosing such an a_0 allows the terms to balance. This causes the peripheral resistance, through the time constant, to directly drive the diastolic pressure, and hence the systolic pressure. This explains the choice of $a_0 = 9$ ms/mmHg by deBoer et al.[5] and subsequently the choice of $a_2 = 1, a_3 = 2, a_4 = 3, a_5 = 2, a_6 = 1$ and $b_2 = 2, b_3 = 4, b_4 = 6, b_5 = 4, b_6 = 2$, all with units ms/mmHg.

Nondimensionalising we put

$$\begin{gathered} S'_n = \tfrac{S_n}{S_0} \quad \hat{S}'_n = \tfrac{\hat{S}_n}{S_0} \quad T'_n = \tfrac{T_n}{T_0} \\ I'_n = \tfrac{I_n}{T_0} \quad F' = \tfrac{F}{S_0} \end{gathered} \tag{2.20}$$

and dropping the primes the equations become

$$\begin{aligned} I_n &= \alpha_0 \hat{S}_n + \sum_{k>0} \alpha_k \hat{S}_{n-k} + \kappa \\ \hat{S}_n &= \frac{1}{S_0} Y(S_n S_0) \\ &= y(S_n) \text{ by definition say} \\ T_n &= 1 - 2\sum_{k>0} \alpha_k \hat{S}_{n-k} \\ S_{n+1} &= \frac{D_0}{S_0} S_n \exp\left\{ -\left[\frac{I_n}{T_n}\right] \right\} + \mu I_n + \nu + F \end{aligned} \tag{2.21}$$

where

$$\alpha_k = \tfrac{a_k S_0}{T_0} \quad \kappa = \tfrac{I_0}{T_0} \quad \mu = \tfrac{\gamma T_0}{S_0} \quad \nu = \tfrac{P_0}{S_0} \tag{2.22}$$

We follow deBoer et al. [5] and take

$$\hat{S}_n = \hat{S}_0 + 18 \tan^{-1}\left(\frac{S_n - 1}{18}\right) \tag{2.23}$$

giving a sigmoidal response curve as in fig. 2.6 centred about $\hat{S}_0$. Substituting typical values gives

$$\alpha_0 \sim 0.76 \quad \alpha_k \lesssim 0.25 \quad \kappa \sim 0.56$$

$$\frac{D_0}{S_0} \sim 0.625 \quad \mu \sim 0.19 \quad \nu \sim 0.73$$

which justifies including all the terms in the model.

Let us now consider the simplified problem with zero forcing, *i.e.* $F = 0$, and $\alpha_k = 0,\ k > 0$, which gives

$$\begin{aligned} I_n &= \alpha_0 \hat{S}_n + \kappa \\ T_n &= 1 \\ S_{n+1} &= \frac{D_0}{S_0} S_n \exp - \left[\frac{I_n}{T_n}\right] + \mu I_n + \nu \\ &\simeq \xi S_n (1 - \alpha_0 S_n) + \nu \end{aligned} \tag{2.24}$$

where $\xi = \frac{D_0}{S_0} e^{-\kappa}$. This gives the fixed points for S, $S^\star$, as 0.79 and -2.59, with only the first value having any physiological sense. We see that $S^\star = 0.79$ is a stable steady state provided ξ is small enough (as it is here), specifically if

$$\xi |1 - 2\alpha_0 S^\star| < 1 \tag{2.25}$$

In the absence of forcing, this steady state can be expected to occur also for non-zero $\alpha_k,\ k > 0$.

2.2.4 Comparison of model with real data

The real system contains noise and is forced by respiration with a frequency $\sim$ 0.3 Hz. In order to compare the output of this system with real data, the respiratory forcing is added to the pulse pressure with amplitude 3 mmHg and frequency 0.3 Hz, eqn 2.15, and Gaussian noise is added to R-R interval and pulse pressure, the right hand sides of eqns. 2.13 and 2.15. Typical output (fig. 2.7) and power spectra of data from the model (fig. 2.8) are comparable to those for real data. The waveforms of the heart rate and blood pressure are similar to those seen in the original data and the power spectra also have similar forms, with the peaks corresponding to baroreceptor reflex response and respiration present. There is no peak at $\sim$ 0.02 Hz in the model

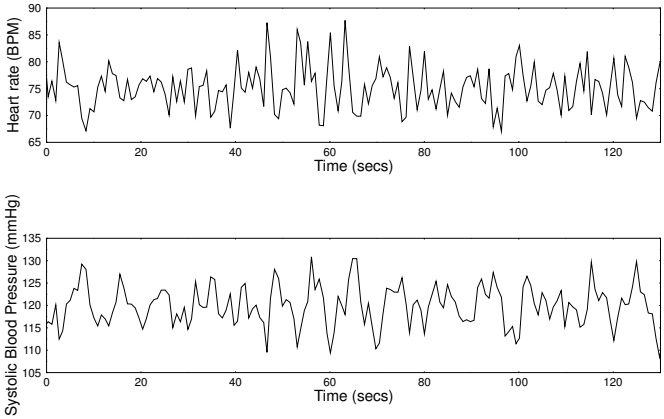

Figure 2.7: Data from the discrete model

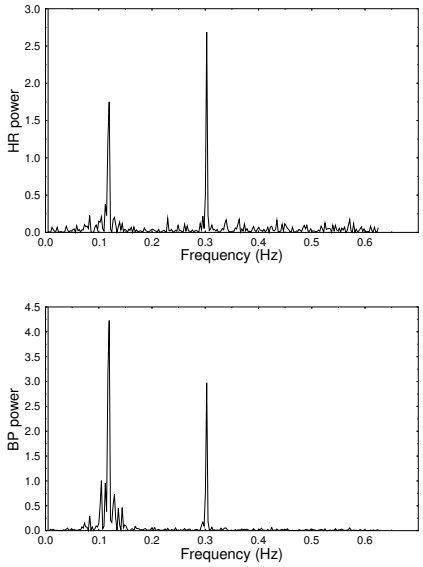

Figure 2.8: Power spectra for the discrete model

data power spectra since the adjustment of the cardiovascular system to changes in surroundings is not considered important, and so is not included in the model. Low level power throughout the spectrum is present from the noise, as is seen in the original data (fig. 2.2). These similarities suggest that for these parameter values the system of difference delay equations successfully models the aspects of the real system which we consider to be important.

In the model the respiratory forcing is added to the blood pressure although it is thought to be forcing the vagus physiologically [1, 10, 16]. Also, the model ceases to give reasonable results for R-R intervals corresponding to heart rate above 75 BPM.

This is due to the rapid reaction of the vagal response. When the heart rate increases the response signal induced in the vagal nerve ceases to affect the current R-R interval, affects the next interval instead, and the R-R equation no longer holds.

The balance between terms in eqn 2.18, as shown in eqn 2.19, causes the peripheral resistance to drive the diastolic pressure directly. This choice of a_0 to balance the terms proves essential, and it is found that the model does not mimic the physical system for other choices of a_0.

2.2.5 Determining the BRS

By altering the parameter values in the model we find that the peaks in the power spectra at 0.3 Hz are due to the respiratory forcing of the pulse pressure, eqn 2.15, with the frequency of respiration concurrent to the frequency at which the peaks occur. The peaks in the power spectra at 0.1 Hz cannot be found to be similarly connected to any parameter. When there is noise present but no respiratory forcing the noise in the 0.05-0.15 Hz frequency range is amplified. With respiratory forcing the power in this range remains unchanged. This shows that in the model the respiratory forcing is not the cause of the 0.1 Hz peak, but there is no way of easily verifying this result for the physical system.

The power of the forcing frequency is modulated in both the R-R interval and blood pressure spectra, fig 2.7, although to different degrees. Consider forming plots of the power at the forcing frequency for R-R interval and systolic blood pressure, by varying the forcing frequency in the model. We may calculate the gain in R-R interval and systolic blood pressure power due to the forcing, see fig. 2.9. Taking the ratio of the gains we recover the gain of the system as defined by eqn 2.9, shown in fig. 2.9. Taking the square root of the gain of the system will give a measure of the baroreceptor reflex sensitivity, since the change in R-R interval power results from the response of the baroreceptor reflex to the change in systolic pressure power.

The estimate obtained for the BRS in this way is a function of forcing frequency, which takes a value $\sim 18 = a_0 + \sum_{k>0} a_k$ for small frequencies and a value of $\sim 9 = a_0$ for frequencies in the range 0.25-0.3 Hz. The variation in the BRS with frequency is explained by the cancelling of sympathetic effects at larger frequencies (>0.15 Hz.), leaving only the effect of the vagal nerve [1, 16]. Rapid variation in the range 0.05-0.15 Hz is due to the nature of the baroreceptor reflex amplification of signals in this range. Assuming that the model gives results similar to the physical system this suggests that a superior way of measuring the gain is to ask patients to breathe metronomically over a range of prescribed frequencies, preferably 0.25-0.3 Hz, since these frequencies are physiologically realisable and the baroreceptor reflex appears to reach a constant

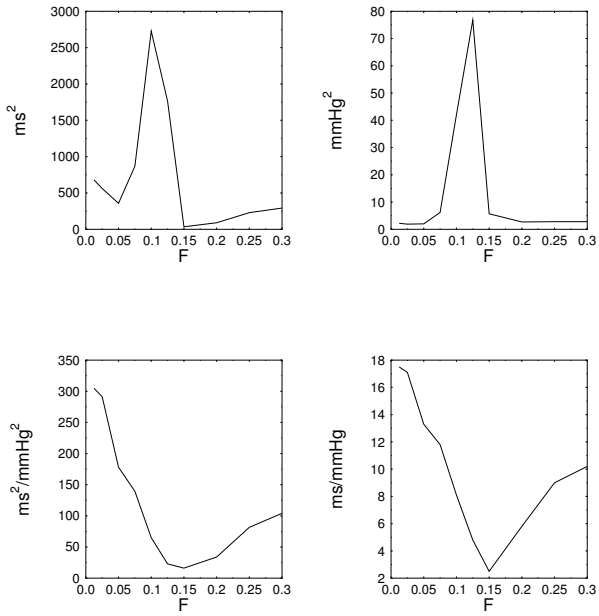

Figure 2.9: Gain for R-R interval (upper left), systolic pressure (upper right), of system (lower left) and square root of gain (lower right)

response sensitivity.

The heart rate and blood pressure data collected in this way may be analysed to find the power at the forcing frequency, and a similar power vs. forcing frequency diagram may be constructed. The change in heart rate and systolic pressure power may be taken as absolute values, since for the model the power at the frequencies concerned were insignificant when no respiratory forcing was present. The average value of the square root of the gain over the range 0.25-0.3 Hz may then be taken as an approximation of the BRS of the vagal nerve.

Chapter 3

SVD Techniques

The Fourier techniques described in section 2.1.2 involve Fourier transforming the time series, constructing their power spectra and then finding the gain and coherence. If the coherence exceeds 0.5 over the range 0.05-0.15 Hz then the average gain in this range is accepted as an approximation to the BRS. Here we look at a generalisation of these Fourier techniques based on singular value decomposition (SVD).

3.1 Time delay embedding

SVD methods are based on the signal processing work of Bertero and Pike [3] and use results from Takens' work [17]. The SVD methods use time delay embedding in order to construct a phase portrait from a given N point time series, $\xi(t) = \{\xi_k\}_{k=1}^{N}$. Choosing a time lag Δ we may construct a d_E-dimensional phase space with basis $\{\xi(t), \xi(t-\Delta), \ldots, \xi(t-(d_E-1)\Delta)\}$. The time series trajectory is embedded in the phase space as the vectors

$$\Xi_k = [\xi_k,\ \xi_{k-\Delta},\ \xi_{k-2\Delta},\ \ldots,\ \xi_{k-(d_E-1)\Delta}] \qquad k = 1, \ldots, M \tag{3.1}$$

$$M = N - d_E + 1$$

where $\xi_j \equiv \xi(t_j)$, to form a d_E-dimensional phase portrait. This embedding may be represented using an $M \times d_E$ trajectory matrix

$$A = \begin{bmatrix} \hat{\Xi}_1^T \\ \hat{\Xi}_2^T \\ \vdots \\ \hat{\Xi}_{d_E}^T \end{bmatrix} \tag{3.2}$$

with $\hat{\Xi}_k$ the normalised k^{th} embedded vector, $\frac{1}{\sqrt{M}}\,\Xi_k$.

Takens proved [17] that for a large enough embedding dimension the embedded trajectory is a good representation of the original system. The choice of time lag, Δ, is also important [9]. Together the time lag and embedding dimension need to allow the distinct points of the time series to separate sufficiently without becoming so disparate that information is lost. Consider embedding the time series generated by a sinusoidal oscillator with period T. For a $d_E = 2$ embedding, the time lags of $\Delta = 0, T/4, T/2$ yield very different embedded trajectories (fig. 3.1). A time lag of zero

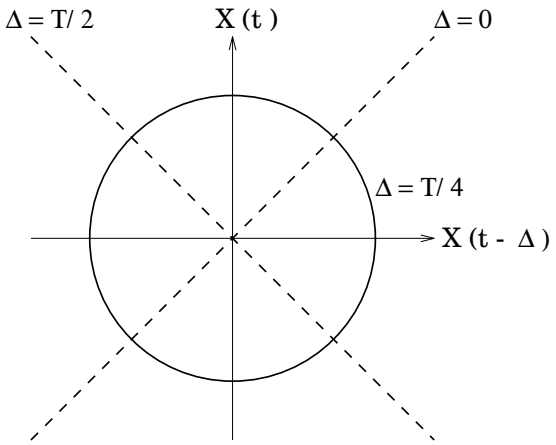

Figure 3.1: 2D embeddings of a sinusoidal oscillator

does not allow the points to separate at all, $T/4$ gives an embedded trajectory with the full two dimensional nature of the oscillator, while $T/2$ is too large and the information is lost, leading to collapse of the trajectory onto one dimension. More generally, if the embedding dimension and time lag are chosen to satisfy

$$\Delta = \frac{T}{2d_E} \tag{3.3}$$

then the embedding will usually retain the full dimensional nature of an oscillator with period T [7]. In the embeddings below the time lag has been chosen to be the sampling interval of the time series, 0.25 seconds, and the embedding dimension has been varied to satisfy eqn 3.3.

3.2 SVD filter method

Having chosen suitable time lag and embedding dimension the time series is embedded using time delay embedding. We then appeal to singular value decomposition (SVD) methods, as developed by Broomhead and King [4] and refined by Vautard and Ghil [18] for use with short, noisy, discrete time series arising from experimental data. SVD involves forming a $d_E \times d_E$ covariance matrix, C, from the trajectory matrix, A, formed during time delay embedding, with

$$C = A^T A \tag{3.4}$$

By solving the eigenvalue problem

$$C\hat{v}_i = \lambda_i \hat{v}_i \tag{3.5}$$

we are able to find the eigenvalues λ_i and corresponding normalised eigenvectors, $\hat{v}_i$ of the covariance matrix C. If we consider embedding the time series using a d_E-dimensional embedding to give a cloud, or mass, of points in R^{d_E} then the eigenvectors give the principal axes of the mass of points, in that the sum of the squares of deviations of the points from each vector is minimised, *i.e.* the eigenvectors are the principal axes in the least squares sense. We now have a set of eigenvectors on which a mass of points are centred, due to the normalisation of the eigenvectors. Consider a mass which is equally spread in a cylindrical region. Then the principal axes are the longitudinal and radial axes of the cylinder. In order to fully describe the mass we also need to know how far along each axis the mass spreads; this is measured by the corresponding eigenvalues.

The eigenvectors are known as *singular vectors* while $s_i = \sqrt{\lambda_i}$ are the corresponding *singular values*, ordered in decreasing magnitude. Choosing a subset of singular vectors as the basis of a new phase space we may project the mass of points onto this phase space, thus filtering out the part of the embedded trajectory corresponding to the singular vectors forming the basis. If the embedding dimension chosen is larger than that of the underlying attractor of the system the singular values will decrease to a constant value. (For clean systems with no noise they will decrease to zero.) These singular values and corresponding singular vectors are discarded, with the remaining set of singular vectors forming the Empirical Orthogonal Functions (EOFs). For experimental data this filters out any noise which has Gaussian distribution, *i.e.* noise normally distributed with mean zero, *e.g.* white noise as arises when recording the data, by virtue of the least squares nature of determining the singular values.

Having filtered the embedded trajectory it is possible to invert the embedding to construct the filtered time series, to which Fourier techniques may be applied as before.

3.2.1 Application to data

We wish to use the SVD filter method to filter the time series so that application of the Fourier techniques described in section 2.1.2 yields results which satisfy the conditions of local linearity, in order that the average gain over the range 0.05-0.15 Hz may be accepted as an approximation to the BRS. The original data used is non-stationary since it contains long term oscillations due to low-frequency (< 0.1 Hz.) variations. These variations result in peaks in the power spectra overlapping in the mid-frequency range (0.05-0.15 Hz.) in which we are interested. Using the SVD filtering method with time lag $\Delta = 0.25$ seconds and $d_E = \frac{T}{2\Delta} = \frac{25}{2*0.25} = 50$, we are able to filter out this non-stationarity by projecting the embedded trajectory onto the first singular vector (corresponding to the largest singular value). The non-stationarity is clearly seen in the filtered time series and corresponding power spectra (fig. 3.2). By taking the residual

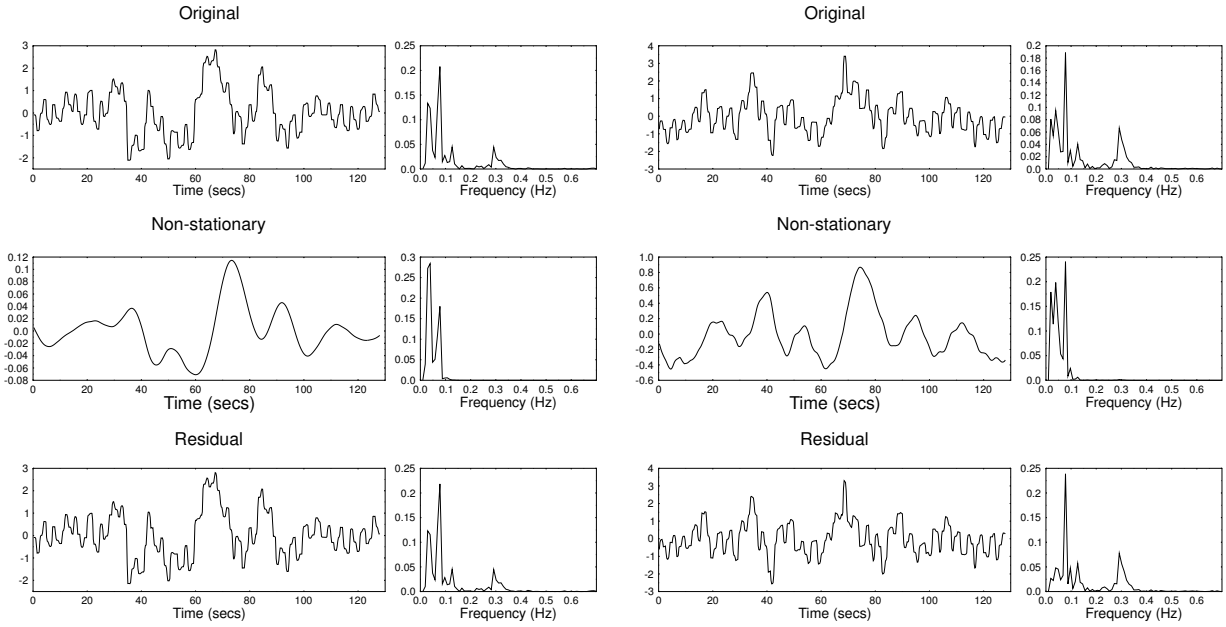

Figure 3.2: SVD filtering with $d_E = 50$, $\Delta = 0.25$ s, patient 5(2) : (a) heart rate and (b) systolic blood pressure

part of the filtered embedding and inverting we have the time series with the non-stationarity removed, and relatively free from white noise. Using SVD to filter in this way is comparable to applying a moving average, although the SVD filter is able to filter out a narrower frequency band by virtue of being optimal in the least squares sense.

A further SVD filter may then be applied, using an embedding with time lag $\Delta = 0.25$ seconds and $d_E = \frac{10}{2*0.25} = 20$. Projection onto different sets of singular vectors shows

that the power in the baroreceptor reflex frequency range, 0.05-0.15 Hz., resides in points lying in the plane of the first three singular vectors. The points corresponding to the third vector also contain most of the power in the respiratory frequency range. In order to obtain the time series with power only in the baroreceptor reflex range we choose to filter by projecting onto the first two singular vectors only, fig. 3.3. By inverting

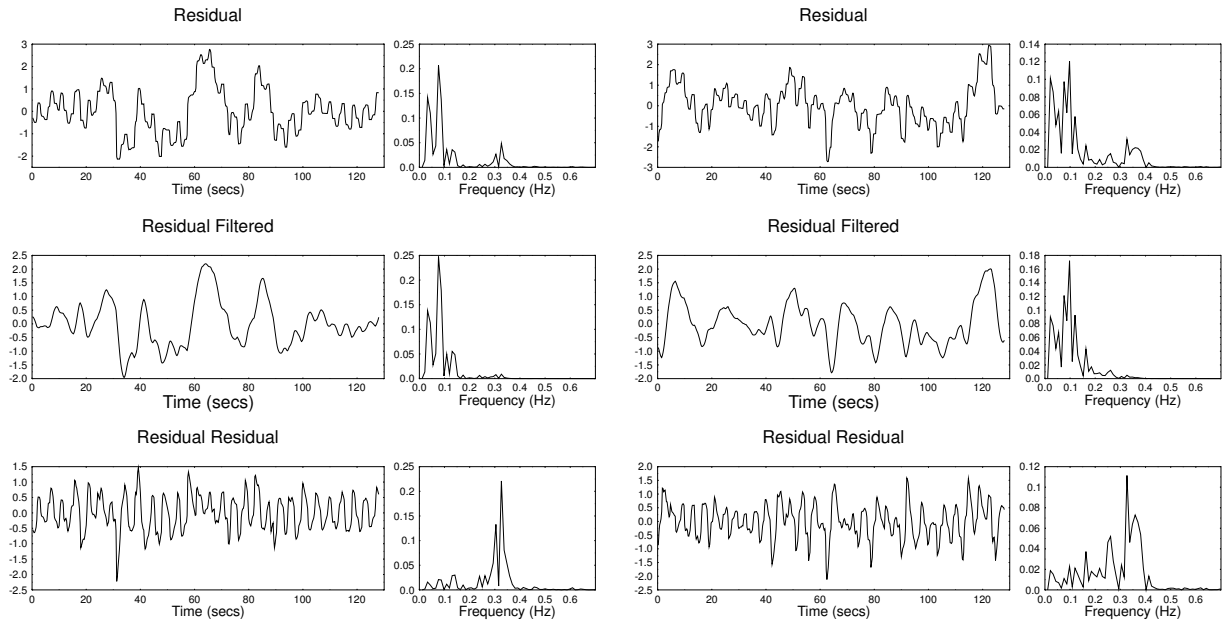

Figure 3.3: SVD filtering of residual with $d_E = 20$, $\Delta = 0.25$ s, patient 5(2) : (a) heart rate and (b) systolic blood pressure

to obtain the corresponding filtered residual time series we are able to apply Fourier techniques as described in section 2.1.2, giving power spectra as in fig. 3.3. Plots of the gain, fig. 3.4 are found to be smoother.

Taking the correlation of the power spectra of the phase shifted series is not robust, since the correlation is radically modified by small shifts in the power spectrum. Although transforming does remove any measure of phase, it also introduces aliasing and leakage which cause splitting of power between neighbouring frequency ranges. This splitting can be seen clearly in the 0-0.05 Hz range of the power spectrum for original systolic pressure in fig. 3.2, and also occurs in the baroreceptor reflex frequency range. A more robust approach to measuring the coherence between the two time series is to eliminate the phase shift in the data by maximising the cross-correlation [2],

$$c_k = \frac{\sum_{t=0}^{N-k}(\phi_t - \mu_\phi)(\psi_{t+k} - \mu_\psi)}{\sqrt{\sum_{t=0}^{N-k}(\phi_t - \mu_\phi)^2 \sum_{t=0}^{N-k}(\psi_t - \mu_\psi)^2}} \tag{3.6}$$

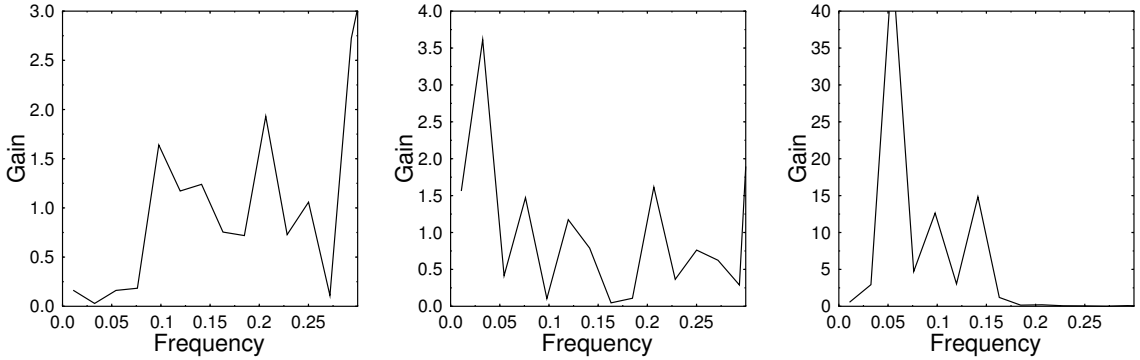

(a) (b) (c)

Figure 3.4: Gain for (a) patient 5(1), (b) patient 5(2) and (c) patient 6

where ϕ = heart rate and ψ = systolic blood pressure, and defining the square, c_k^2, to be the coherence of the two series. The coherence defined in this way yields results which are larger than the average coherence found using Fourier techniques, cf. fig. 2.4.

3.3 Comparison with Fourier method

This method uses SVD methods to filter out the part of the time series which contains the data in which we are interested. This gives cleaner data which leads to smoother plots of gain. The improved method of measuring correlation and cleaner data together give values for the coherence which exceed the required 0.5 level for some of the data, *e.g.* patient 5(2), and so the average gain may be accepted as an approximation to the BRS, see section 2.1.4.

Although the filtered data shows sufficient linearity in coupling between the heart rate and blood pressure to justify using the preservation of linear relations by Fourier techniques, we still require justification that the gain over the range 0.05-0.15 Hz. is an approximation to the BRS.

We wish to find the sensitivity of the baroreceptor reflex. The traditional pressor drug method, as described in section 1.3, seeks to do this by measuring the response in heart rate to a known change in blood pressure, and assumes reasonably that this response arises through the coupling of heart rate and blood pressure via the baroreceptor reflex. Let us make the assumption that changes in heart rate and blood pressure are small fluctuations about the mean so that the gain may be considered a measure of the square

of the ratio of change in heart rate to change in blood pressure, *i.e.*

$$\text{gain}(f) \propto \left| \frac{\text{change in heart rate}}{\text{change in blood pressure}} \right|^2 \tag{3.7}$$

Then the gain may be considered to be a measure of the sensitivity of the baroreceptor reflex *only* if the change in heart rate is due to the effect of the baroreceptor reflex response to the corresponding change in blood pressure. Thus the method relies on the assumption that the fluctuations with frequencies in the range 0.05-0.15 Hz in the heart rate power spectrum are caused by the effect of signals emitted by the baroreceptor reflex. Further, it assumes that any baroreceptor reflex response is induced by a change in the blood pressure whose frequency also lies in the range 0.05-0.15 Hz.

There is evidence that the fluctuations induced in the heart rate by the signals emitted by the baroreceptor reflex do have frequencies in the range 0.05-0.15 Hz, as can be seen in the power spectra of the original data, see fig. 2.3. The weak coupling between the heart rate and blood pressure causes the blood pressure data to have power in this frequency range also. However, there is no evidence, nor is there any reason to suppose, that the fluctuations in blood pressure which induce a response from the baroreceptor reflex have frequencies in the range 0.05-0.15 Hz.

The use of the knowledge that the baroreceptor reflex response is the emission of signals with frequencies in the range 0.05-0.15 Hz seems to have been incorrectly applied, and we now seek to develop an alternative, non-invasive method of estimating the sensitivity of the baroreceptor reflex.

Chapter 4

Frequency response and a continuous model of the CVS

We have shown that the method currently used may be improved by using SVD methods, but it is not justified in providing an approximation to the BRS. Here we look at a model which has results comparable to those of the cardiovascular system (CVS) for a large range of parameter values in order to determine if plotting the frequency response, as suggested in section 2.2.3, is a viable way of finding an approximation to the BRS. We consider a continuous closed loop model of the CVS, based on the model developed by Madwed, Albrecht, Mark and Cohen [12].

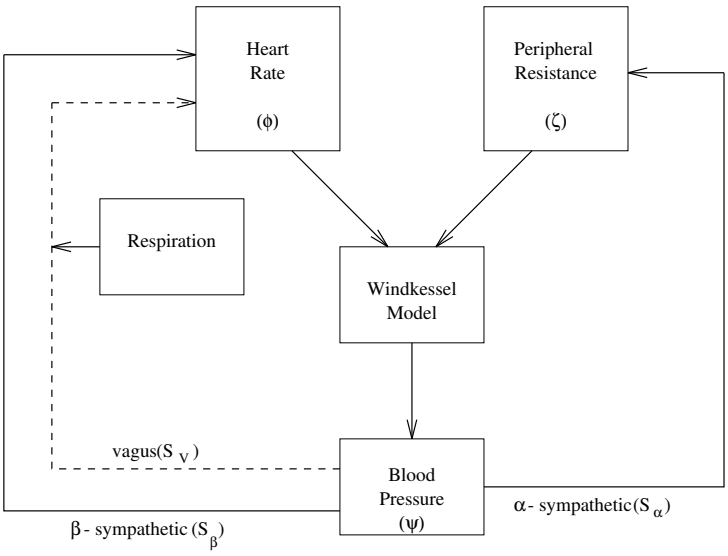

Figure 4.1: Diagram of the continuous model

The model consists of three response variables - heart rate ϕ, blood pressure ψ and peripheral resistance ζ, which are regulated by the 'controllers' S_α, S_β and S_V which represent the activity levels of the α and β- sympathetic and vagal nerves. Clinical study demonstrates that the CVS appears to be operating as a closed negative feedback loop [8] with the sympathetic nervous system exhibiting a delayed response and the vagal nerve response being almost instantaneous which we wish to reflect in the model.

The vagal nerve acts to decelerate the heart rate while the β-sympathetic acts to accelerate the heart rate, which is thus modelled by

$$\phi = \delta S_\beta - \gamma S_V \qquad\qquad (\delta, \gamma) > 0 \tag{4.1}$$

The α-sympathetic nerve acts to alter the peripheral resistance, modelled as

$$\zeta = f_\zeta(\zeta, S_\alpha) \tag{4.2}$$

where f_ζ is the response curve of the peripheral resistance. The blood pressure induces changes in the activity levels, causing changes in the heart rate and peripheral resistance which in turn affect the blood pressure. Experimental data is found to be described by the Windkessel model as in section 2.2.2, given by

$$\psi = \psi_0 \exp\left[\frac{-1}{b\phi\zeta}\right] \exp\left[\frac{1}{b\phi_0\zeta_0}\right] \qquad (b > 0) \tag{4.3}$$

The controllers respond to the blood pressure, via the baroreceptor reflex, with differing speeds of reaction. The changes in the slower reacting sympathetic nerves depend on the blood pressure and also on the present activity level. They are modelled by

$$\dot{S}_\beta = -\epsilon_\beta S_\beta - f_\beta(\psi_{\tau_\beta}) \qquad\qquad \psi_{\tau_\beta} = \psi(t - \tau_\beta) \tag{4.4}$$

$$\dot{S}_\alpha = -\epsilon_\alpha S_\alpha - f_\alpha(\psi_{\tau_\alpha}) \qquad\qquad \psi_{\tau_\alpha} = \psi(t - \tau_\alpha) \tag{4.5}$$

while the vagal activity is represented as

$$S_V = f_V(\psi) \tag{4.6}$$

where the fs represent the response curves of the different nerves to the blood pressure, as in eqn. 2.12. In order to compare this model to the real system we will need to include respiratory forcing and white noise. The respiratory forcing, f_{resp}, is added to the vagal controller, as is thought to be the case physiologically [12], while white noise is added to the heart rate. Following Madwed et al. [12] we take the response curves

$$f_x(y) = a_x \tanh(b_x y) \tag{4.7}$$

Thus we have a system of six equations governing the three response variables and the three controllers considered to be vital to the coupling of the heart rate and blood pressure via the baroreceptor reflex:

$$\phi = \delta S_\beta - \gamma S_V + \text{noise} \qquad (\delta, \gamma) > 0$$

$$\zeta = a_\zeta \tanh(b_\zeta S_\alpha)$$

$$\psi = \psi_0 \exp\left[\frac{-1}{b\phi\zeta}\right] \exp\left[\frac{1}{b\phi_0\zeta_0}\right] \qquad (b > 0)$$

$$\dot{S}_\beta = -\epsilon_\beta S_\beta - a_\beta \tanh(b_\beta \psi_{\tau_\beta}) \qquad \psi_{\tau_\beta} = \psi(t - \tau_\beta)$$

$$\dot{S}_\alpha = -\epsilon_\alpha S_\alpha - a_\alpha \tanh(b_\alpha \psi_{\tau_\alpha}) \qquad \psi_{\tau_\alpha} = \psi(t - \tau_\alpha)$$

$$S_V = a_V \tanh(b_V \psi) + f_{resp}$$

4.1 Simple model

Before dealing with the full model we first consider a reduced system which contains the main characteristics of the control variables described above. Obviously we need to include a negative delay feedback. Considering the second term in the sympathetic controller equations, and writing ψ in terms of S_α and S_β, we find that we may represent the main characteristcs by

$$\dot{X} = -\epsilon X - f(X_\tau) + F \tag{4.8}$$

where F is a forcing term comprised of an oscillatory term (respiration) and white noise and $f(X_\tau) = a \tanh[X(t - \tau)]$. This may be linearised for *small fluctuations* giving

$$\dot{X} \approx -\epsilon X - aX(t - \tau) + F \tag{4.9}$$

In order to analyse the stability of the system we ignore forcing and substitute $X = e^{\lambda t}$ into the above linearised equation to get

$$\lambda = -\epsilon + ae^{-\lambda\tau} \tag{4.10}$$

Putting $\lambda = u + iv$ and equating the real and imaginary terms:

$$\begin{aligned} u &= -\epsilon + ae^{-u\tau}\cos(v\tau) \\ v &= -ae^{-u\tau}\sin(v\tau) \end{aligned} \tag{4.11}$$

For oscillatory instability, we choose $u = 0$ giving

$$\begin{aligned} \epsilon &= a\cos(v\tau) \\ v &= -a\sin(v\tau) \end{aligned} \tag{4.12}$$

and this implies that

$$\tan(v\tau) = \frac{-v}{\epsilon} \tag{4.13}$$

which are hence the resonance locations. Putting $Y = v\tau$ we have

$$\tan Y = \frac{-Y}{\epsilon\tau} \tag{4.14}$$

Typical values of the delays τ_α and τ_β are 5 s and 2.5 s respectively, while $\epsilon_\alpha \sim 0.15$ and $\epsilon_\beta \sim 0.3$. Taking the α-sympathetic parameters $\epsilon \approx 0.15$ and $\tau \approx 5$ we have $\epsilon\tau \sim 1$ which gives $Y \sim 2$ and $v \sim \frac{2}{\tau}$. Squaring eqn 4.12 and substituting $v \sim \frac{2}{\tau}$ gives

$$\epsilon^2 + \frac{4}{\tau^2} = a^2 \tag{4.15}$$

which, assuming $\epsilon^2 \ll 4/\tau^2$, gives

$$a \sim \frac{2}{\tau} \tag{4.16}$$

For the values of ϵ and τ above this gives $a \approx 0.4$. From data output from a computer implementation of the above model, data is collected and processed as described in 2.1.2. Repeating this process for different forcing frequencies F we may construct power vs. forcing frequency plots, see fig. 4.2. This shows $a \approx 0.4$ to be a resonant location.

If we assume X *decays* for $t \to \infty$ and $X = 0$, $t \leq 0$ then a Fourier transform of eqn 4.9 gives,

$$-i\omega\bar{X} \approx -\epsilon\bar{X} - a\exp(i\omega\tau)\bar{X} + \bar{F} \tag{4.17}$$

$$\bar{X} \approx \left[\frac{1}{\epsilon - i\omega + ae^{i\omega\tau}}\right]\bar{F} \tag{4.18}$$

The gain at the forcing frequency, is given by

$$\begin{aligned} G_R &= \frac{|\bar{X}|^2}{|\bar{F}|^2} \\ &\approx \frac{1}{(\epsilon + a\cos\omega\tau)^2 + (a\sin\omega\tau - \omega)^2} \end{aligned} \tag{4.19}$$

and may be plotted for various forcing frequencies to give a *frequency response*. To verify 4.19 we compare the exact and predicted frequency responses for $\epsilon = 0.1, \tau = 2.0, a = 0.8$

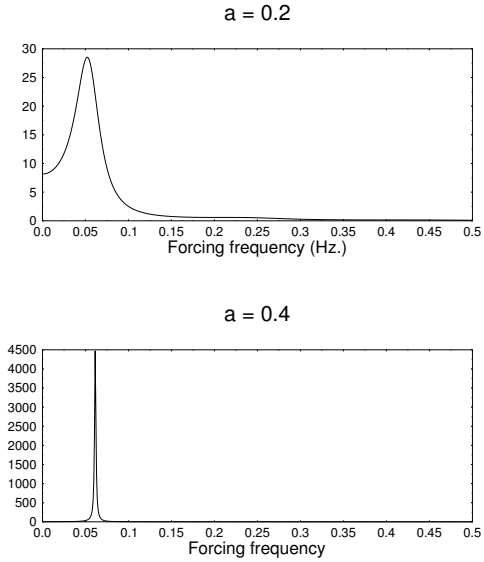

Figure 4.2: Power spectra of simple model for $\epsilon = 0.15, \tau = 5$ and $a = 0.2$, 0.4

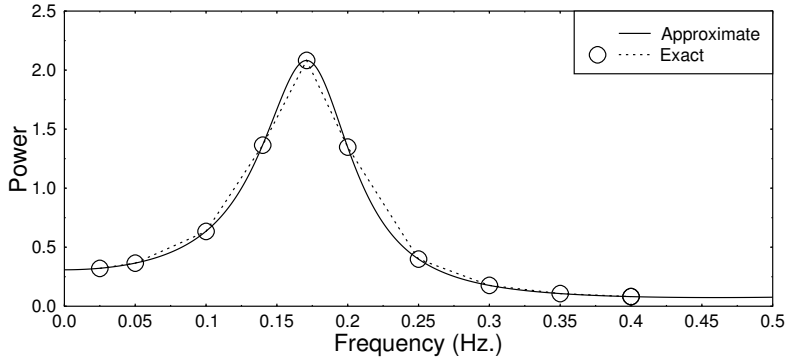

Figure 4.3: Exact and approximate frequency response to small forcing

(see fig. 4.3) and find them to be in agreement. To examine the frequency response for more realistic parameters we choose $\epsilon = 0.15$, $\tau = 5$, corresponding to α-sympathetic parameter values, and consider eqn. 4.19 for various values of a (see fig. 4.2). The model varies from low frequency response with period of 4τ ($a = 0.2$) to resonance ($a \sim 0.4$). By examining eqn. 4.19 and using the knowledge that $G_R \to \infty$ at the resonant frequency, we have

$$\tan(\omega\tau) = \frac{-\omega}{\tau} \tag{4.20}$$

independent of a and ϵ. For $\tau = 5$ we find $\omega \approx 0.4$ and hence $f = \frac{\omega}{2\pi} \approx 0.06$ as in agreement with 4.2. The simple model suggests that the delay difference equations are

acting as bandpass amplifiers, amplifying signals which fall into a specified frequency range.

4.2 Frequency response of full model

We now analyse the full model to find its frequency response. The data output from the model, which are deviations from typical values, is comparable to that of the real system, see fig. 4.4.

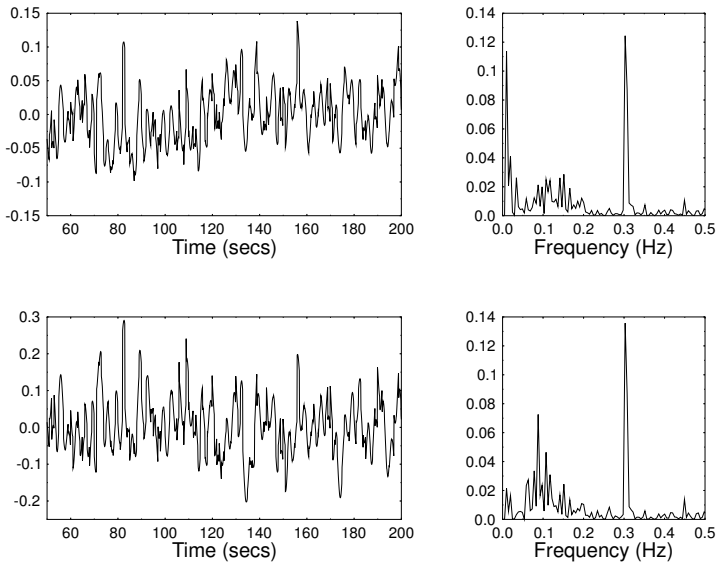

Figure 4.4: Data (left) and power spectra (right) for heart rate (upper) and blood pressure (lower) from the continuous model

Nondimensionalising we put

$$\psi' = \frac{\psi}{\psi_0} \quad \phi' = \frac{\phi}{\phi_0} \quad \zeta' = \frac{\zeta}{\zeta_0} \tag{4.21}$$

and then drop the primes. The response equations become

$$\begin{aligned} \phi &= \delta' S_\beta - \gamma' S_V \\ \zeta &= a'_\zeta \tanh(b_\zeta S_\alpha) \\ \psi &= \exp\left[-\tfrac{1}{b'}\left(\tfrac{1}{(1+\phi)(1+\zeta)} - 1\right)\right] - 1 \end{aligned} \tag{4.22}$$

and the control equations become

$$\begin{aligned}
\dot{S}_\beta &= -\epsilon_\beta S_\beta - a_\beta \tanh\left[b'_\beta \psi_{\tau_\beta}\right] \\
\dot{S}_\alpha &= -\epsilon_\alpha S_\alpha - a_\alpha \tanh\left[b'_\alpha \psi_{\tau_\alpha}\right] \\
S_V &= a_V \tanh\left[b'_v \psi\right] + F
\end{aligned} \tag{4.23}$$

where

$$\begin{gathered}
\delta' = \tfrac{\delta}{\phi_0} \qquad \gamma' = \tfrac{\gamma}{\phi_0} \qquad a'_\zeta = \tfrac{a_\zeta}{\zeta_0} \qquad b' = b\phi_0\zeta_0 \\
b'_\beta = b_\beta\psi_0 \quad b'_\alpha = b_\alpha\psi_0 \quad b'_V = b_V\psi_0
\end{gathered} \tag{4.24}$$

Typical values of these parameters are not easily attainable from experimental data. Following Madwed et al. [12] we use this set of non-dimensional equations in implementing the program to obtain the results as shown in fig. 4.4, with parameter values

$$\delta' = 0.5 \quad \gamma' = 0.5 \quad a'_i = 1.0 \quad b'_i = 0.5 \tag{4.25}$$

For small fluctuations this nondimensional set of equations is easily linearised, and dropping the primes on the constants we have

$$\begin{aligned}
\phi &= \delta S_\beta - \gamma S_V \\
\zeta &= d_\zeta S_\alpha \\
\psi &\sim \exp\left[\frac{-1}{b}\left([1-\phi][1-\zeta]-1\right)\right] - 1 \\
&\sim \exp\left[\frac{-1}{b}\left(1-(\phi+\zeta)+\ldots-1\right)\right] - 1 \\
&\sim \frac{\phi+\zeta}{b} \\
\dot{S}_\beta &= -\epsilon_\beta S_\beta - d_\beta \psi_{\tau_\beta} \\
\dot{S}_\alpha &= -\epsilon_\alpha S_\alpha - d_\alpha \psi_{\tau_\alpha} \\
S_V &= d_V \psi + F
\end{aligned} \tag{4.26}$$

where $a_\zeta b_\zeta = d_\zeta$ *etc.*

Assuming that all the variables are identically zero for $t \leq 0$ and decay as $t \to \infty$ we can take Fourier transforms to get

$$\begin{aligned}
\bar{\phi} &= \delta \bar{S}_\beta - \gamma \bar{S}_V \\
\bar{\zeta} &= d_\zeta \bar{S}_\alpha \\
\bar{\psi} &\sim \frac{1}{b}(\bar{\phi} + \bar{\zeta}) \\
\bar{S}_\beta &= \frac{1}{g_\beta}\bar{\psi} \\
\bar{S}_\alpha &= \frac{1}{g_\alpha}\bar{\psi} \\
\bar{S}_V &= d_V \bar{\psi} + \bar{F}
\end{aligned} \tag{4.27}$$

where

$$g_\alpha = \frac{d_\alpha}{\epsilon_\alpha^2 + \omega^2}[(\cos \omega\tau_\alpha - \omega \sin \omega\tau_\alpha) + i(\epsilon_\alpha \sin \omega\tau_\alpha + \omega \cos \omega\tau_\alpha)] \tag{4.28}$$

and similarly for g_β.

Manipulation then gives

$$-\frac{\bar{\phi}}{\gamma \bar{F}} = \frac{bR_{\alpha\beta} - d_\zeta R_\beta + i(bI_{\alpha\beta} - d_\zeta I_\beta)}{(b + \gamma d_V)R_{\alpha\beta} - d_\zeta R_\beta - \delta R_\alpha + i((b + \gamma d_V)I_{\alpha\beta} - d_\zeta I_\beta - \delta I_\alpha)} \tag{4.29}$$

where $R_\alpha,\ R_\beta,\ R_{\alpha\beta}$ are the real parts of $\bar{f}_\alpha,\ \bar{f}_\beta,\ \bar{f}_\alpha \bar{f}_\beta$ respectively, and similarly the I's are the imaginary parts. Taking the modulus squared gives the equivalent of the gain, and we look (see fig. 4.5) at the frequency response of this gain. The range of values of gain is different from those in fig. 2.9 due to the non-dimensional nature of the equations used to generate the results seen here. Once again the frequency response becomes approximately constant in the frequency range 0.25-0.3 Hz. This verifies that getting patients to breathe metronomically at frequencies within this region, plotting the frequency response and using the average value in the range 0.25-0.3 Hz. would be a suitable way of approximating the BRS, as suggested in section 2.2.3.

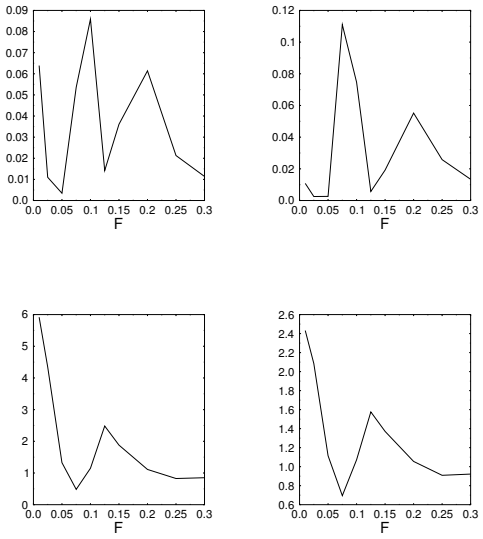

Figure 4.5: Gain of heart rate (upper left), blood pressure (upper right), of system (lower left) and square root of gain (lower right)

4.3 Frequency response of real data

We have suggested an alternative method for determining the BRS, and wish to apply it to real data to see if the method suggested by the models holds for the physiological system. In order to obtain similar conditions to those imposed on the models we require the patient to breathe metronomically, *i.e.* at a fixed freqeuncy, and for the amplitude of the forcing to be constant, which physiologically requires the tidal volume to be constant. This is non-trivial since the tidal volume usually decreases with increasing respiratory rate. However, the use of a ventilator, as used in intensive care units, allows regulation of both the respiratory rate and the tidal volume.

Data was recorded from a healthy patient breathing at 12, 16 and 20 breaths per minute, corresponding to forcing frequencies 0.2, 0.27 and 0.33 Hz, see fig. 4.6. This data was processed as described in section 1.2, although the data for 0.33 Hz was unable to be processed due to large swings in the blood pressure which prevented the peak detection from extracting the systolic blood pressure. From the power spectra, fig. 4.6 we are able to read off the value of heart rate and systolic blood pressure power at the forcing frequency, enabling us to calculate the gain, and the frequency response, *i.e.* the square root of the gain vs. forcing frequency, fig. 4.7.

The frequency response is varying slightly in agreement with the results from the continuous model, see fig. 4.5. Although we only have two values and they are not in the region of constant sensitivity we may take the average value, 4.3 ms/mm Hg,

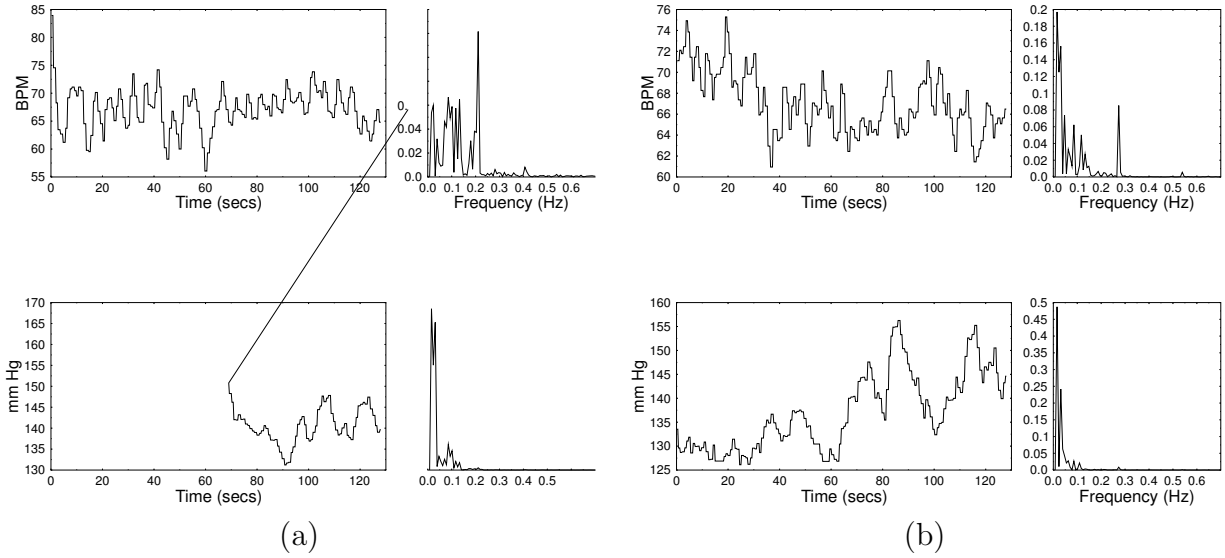

(a) (b)

Figure 4.6: Data and power spectra for heart rate (upper) and blood pressure (lower) for patient 7, respiratory rate (a) 12 and (b) 16 breaths per minute

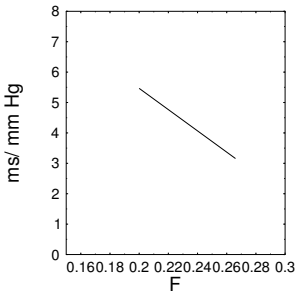

Figure 4.7: Frequency response, *i.e.* the square root of the gain vs. forcing frequency, for patient 7

to approximate the vagal BRS. The BRS is thought be in the range 9-18 ms/mm Hg and the vagal contribution accounts for approximately half of this [5], hence the result obtained is a realistic figure for the vagal contribution to the BRS.

Chapter 5

Concluding Remarks

In this dissertation we have investigated how to determine the baroreceptor reflex sensitivity (BRS) in order to aid doctors in the diagnosis of the cause of hypertension. After outlining the importance of the BRS and explaining how data is obtained we considered the method currently used [15], involving the use of Fourier techniques. Application to several different data sets illustrated the shortcomings of this method.

Looking at a discrete model of the system, developed by deBoer et al. [5] we gained insight into the cardiovascular system. This revealed that the peak in the power spectra in the 0-0.10 Hz range is mainly due to the non-stationarity of the data. An alternative method of calculating an approximation to the BRS was suggested, involving metronomic breathing at various frequencies, although the limited parameter ranges over which the model holds caused us to question whether the results from this model would hold for the physiological system.

In chapter three we applied singular value decomposition (SVD) methods [18] to filter out the non-stationarity in the data and to extract a much cleaner signal, containing data with frequencies in the range 0.05-0.15 Hz. Application of the Fourier techniques from section 2.1.2 to this filtered signal gave improved results which in some cases, *e.g.* patient 5(2), satisfied the conditions for the gain to be accepted as an approximation to the BRS. With our improved knowledge of the cardiovascular system we questioned the validity of the current method to give an approximation of the BRS, and found that the method is ill-founded.

A continuous model, based on that of Madwed et al. [12] is developed which holds for large ranges of parameter values. Simplification yields encouraging results, and progressing to analysis of the full model we obtained results similar to those from the discrete model. Preliminary results obtained by applying this method to real data suggest that this alternative, frequency response method gives an improved approximation to the BRS.

In order to confirm that the frequency response method gives an improved approximation to the BRS, a future aim is to overcome the problems of peak detection and so extend the frequency range over which the data may be obtained. The solution to this problem may lie in constructing a three dimensional graph, with tidal volume as the extra variable. If a library of frequency responses, the square root of gain vs. forcing frequency, can be constructed including data from healthy patients and those with varied, known causes of hypertension, then it may be possible to compare a patient's frequency response with those in the library and so determine the cause of hypertension.

This dissertation does not provide a new method which continuously analyses ECG and blood pressure output to yield a realistic approximation of the BRS, which is the ideal solution which doctors seek. However, we have outlined the faults of the method currently used and used known facts about the cardiovascular system and baroreceptor reflex to construct an alternative, justifiable method of approximating the baroreceptor reflex sensitivity.

Bibliography

[1] S. Askelrod, D. Gordon, J.B. Madwed, N.C. Snidman, D.C. Shannon, and R.J. Cohen. Hemodynamic regulation: investigation by spectral analysis. *Am. J. Physiol.*, 249 H:867–875, 1985.

[2] J.S. Bendat and A.G. Piersol. *Random data: analysis and measurement procedures*. Wiley and Sons, 1986.

[3] M. Bertero and E.R. Pike. Resolution in diffraction - limited imaging, a singular value analysis (1): The case of coherence illumination. *Opt. Acta.*, 29:727–734, 1982.

[4] D.S Broomhead and G.P. King. Extracting qualitative dynamics from experimental data. *Physica D*, 20:217–236, 1986.

[5] R.W. deBoer, J.M. Karemaker, and J. Strackee. Haemodynamic fluctuations and baroreflex sensitivity in humans: a beat-to-beat model. *Am. J. Physiol.*, 253:680–689, 1987.

[6] D.L. Eckberg. Nonlinearities of the human carotid baroreceptor - cardiac reflex. *Circ. Res.*, 47:208–216, 1980.

[7] A.C. Fowler, G. Kember, P. Johnson, S.J. Walter, P. Fleming, and M. Clements. A method for filtering respiratory oscillations. *J. Theor. Biol.*, 170:273–281, 1994.

[8] J.M. Karemaker. Neurophysiology of baroreceptor reflex. In R.I. Kitney and O. Rompelman, editors, *The beat-to-beat investigation of cardiovascular function - Measurement, analysis and applications*, Oxford, 1987. Clarendon Press.

[9] G. Kember and A.C. Fowler. A correlation function for choosing time delays in phase portrait reconstructions. *Phys. Letts. A*, 179(2):72–80, 1993.

[10] L.A. Lipsitz. Age related changes in the complexity of cardiovascular dynamics: A potential marker of vulnerability to disease. *Chaos*, 5(1):102–109, 1995.

[11] M.C. Mackey and L. Glass. Oscillation and chaos in physiological control systems. *Science*, 197:287–289, 1977.

[12] J.B. Madwed, P. Albrecht, R.G. Mark, and R.J. Cohen. Low-frequency oscillations in arterial pressure and heart rate: a simple computer model. *Am. Physiol. Soc.*, 256 H:1573–1579, 1989.

[13] A.V. Oppenheim and R.W. Schafer. *Digital Signal Processing*. Prentice-Hall, 1975.

[14] W.H. Press, B.P. Flannery, S.A. Teukolsky, and W.T. Vetterling. *Numerical Recipes*. CUP, 1986.

[15] H.W.J. Robbe, L.J.M. Mulder, H. Ruddel, W.A. Langewitz, J.B.P. Veldman, and G. Mulder. Assessment of baroreceptor reflex sensitivity by means of spectral analysis. *Hypertension*, 10:538–543, 1987.

[16] J.P. Saul. Beat-to-beat variations of heart rate reflect modulation of cardiac autonomic outflow. *Am. J. Physiol.*, 5:32–37, 1990.

[17] F. Takens. Detecting strange attractors in fluid turbulence. In D. Rand and L.-S. Young, editors, *Dynamical Systems and Turbulence*, pages 366–381, Berlin, 1981. Springer Verlag.

[18] R. Vautard and M. Ghil. Singular spectral analysis in non-linear dynamics, with applications to paleoclimatic time series. *Physica D*, 35:395–424, 1989.